Bundle structures of stretching-energy and nonlinear interactions among modes in elastic wave turbulence

Masanori Takaoka[1] **and Naoto Yokoyama**[2]

[1] Department of Mechanical Engineering, Doshisha University, Kyotanabe 610-0394, Japan
[2] Department of Aeronautics and Astronautics, Kyoto University, Kyoto 615-8540, Japan

E-mail: [1]mtakaoka@mail.doshisha.ac.jp
[2]yokoyama@kuaero.kyoto-u.ac.jp

Abstract.
The real-space dynamics and the nonlinear interactions among Fourier modes in elastic wave turbulence are investigated by simulating the Föppl-von Kármán equation. We find that the bundle structures of ridges appear intermittently in the time evolution of the stretching energy field. The time-evolution of the nonlinearity indicates the existence of active and moderate phases in turbulent state. Conditional sampling analysis reveals that the bundle structure, which is the embodiment of the strong nonlinear interactions among modes, induces the energy supply from an external force to the system.

1. Introduction

Elastic wave turbulence, which is governed by the Föppl-von Kármán (FvK) equation [1], has been studied theoretically, numerically and experimentally, and exhibited rich phenomena. Various energy spectra in statistically steady states have been reported. While the energy spectrum $\mathcal{E}(k) \propto k[\log(k_*/k)]^{1/3}$ predicted by the weak turbulence theory (WTT) is successfully reproduced by simulating the FvK equation in the pioneering work [2], the experiments in [3, 4] show different powers of energy spectra $\mathcal{E}(k) \propto k^0 \sim k^{-0.2}$, where $\mathcal{E}(k)$ is an azimuthally-integrated spectrum and $k = (k_x^2 + k_y^2)^{1/2}$. The dimensional analysis suggests other powers of energy spectrum: $\mathcal{E}(k) \propto k^{-1}$ for energy cascade and $\mathcal{E}(k) \propto k^{-1/3}$ for wave action cascade.

In our previous works [5, 7], we have systematically reproduced the variability of the energy spectra by changing the magnitudes of external forces. We have also found the coexistence of the weak and strong turbulence spectra which exists universally for sufficiently wide inertial range. The analytical expression of the separation wavenumber between them has been proposed and numerically validated for various values of parameters. Recently in Ref. [8], we analyzed energy budget by using energy decomposition that is enabled by a single-wavenumber representation of nonlinear energy spectrum. All the above analyses were done in the Fourier space.

We will report here the properties of elastic wave turbulence in the real space. Examined are the real-space structures and the probability density functions of the decomposed energies in addition to the lateral displacement of a plate. We also performed conditional sampling analysis to distinguish active and moderate phases in turbulent state, which reveals the relation between the bundle structure in the real space and the nonlinear interactions among Fourier modes.

2. Formulation

2.1. Basic equations

To investigate the dynamics of elastic waves, we numerically solved the FvK equation

$$\frac{\partial p}{\partial t} = -\frac{Eh^2}{12(1-\sigma^2)}\Delta^2\zeta + \{\zeta,\chi\}\,, \quad \frac{\partial \zeta}{\partial t} = \frac{p}{\rho}, \quad \Delta^2\chi = -\frac{E}{2}\{\zeta,\zeta\}\,, \tag{1}$$

where η, p and χ are respectively the lateral displacement, the momentum and the Airy stress potential. The Young's modulus E, the Poisson ratio σ and the density ρ are the physical properties of the elastic plate. The thickness of the plate is expressed by h, and $\Delta = \partial_{xx} + \partial_{yy}$ and $\{f,g\} = \partial_{xx}f\partial_{yy}g + \partial_{yy}f\partial_{xx}g - 2\partial_{xy}f\partial_{xy}g$ are the Laplace operator and the Monge-Ampère operator, respectively. We adopted the parameter values of the steel plate used in the experiment which are shown in Ref. [3].

The pseudo-spectral method is employed, since the plate is supposed to have the periodic boundary of 1m×1m. The number of the aliasing-free modes is 256×256, though 512×512 mode is used in the calculation of the convolution. The fourth-order Runge-Kutta method is used for the time integration. The external force and the dissipation, which are respectively localized in low-, $k \le 8\pi$, and high-, $k \gtrsim 256\pi$, wavenumber ranges, are added to achieve statistically-steady non-equilibrium states. The details of the numerical method are explained in Ref. [5].

2.2. Energy decomposition

The energy decomposition is convenient to investigate the energy budget in detail as pointed out in our recent manuscript [8]. The decomposed energies are the kinetic energy K, the bending energy V_b and the stretching energy V_s:

$$K = \frac{p^2}{2\rho}, \quad V_\mathrm{b} = \frac{Eh^2\left((\Delta\zeta)^2 - (1-\nu)\{\zeta,\zeta\}\right)}{24(1-\nu^2)}, \quad V_\mathrm{s} = \frac{(\Delta\chi)^2 - (1+\nu)\{\chi,\chi\}}{2E}. \tag{2}$$

Fourier spectral representation is suitable for the analysis of homogeneous turbulence. We here introduce the Fourier coefficients of ζ, p and χ as $\zeta_{\boldsymbol{k}}$, $p_{\boldsymbol{k}}$ and $\chi_{\boldsymbol{k}}$ respectively. Adoption of $\zeta_{\boldsymbol{k}}$, $p_{\boldsymbol{k}}$ and $\chi_{\boldsymbol{k}}$ as elementary waves enables the single-wavenumber representations of these decomposed energies under the periodic boundary condition:

$$K_{\boldsymbol{k}} = \frac{|p_{\boldsymbol{k}}|^2}{2\rho}, \qquad V_{\mathrm{b}\boldsymbol{k}} = \frac{\rho\omega_{\boldsymbol{k}}^2|\zeta_{\boldsymbol{k}}|^2}{2}, \qquad V_{\mathrm{s}\boldsymbol{k}} = \frac{k^4|\chi_{\boldsymbol{k}}|^2}{2E}, \tag{3}$$

where the frequency $\omega_{\boldsymbol{k}}$ is determined by the linear dispersion relation. We here categorize the former two energies (latter one energy) as linear (nonlinear) energy, since their (its) order of complex amplitudes is quadratic (quartic). Note that adoption of complex amplitudes as elementary waves makes nonlinear energies the convolution of four waves as known in WTT.

3. Numerical Results

3.1. Energy spectra and real-space structures

In Fig. 1 shown are the ensemble averaged azimuthally-integrated spectra of the total energy $\mathcal{E}$, the kinetic energy $\mathcal{K}$, the potential energy $\mathcal{V}$, the bending energy $\mathcal{V}_\mathrm{b}$, the stretching energy $\mathcal{V}_\mathrm{s}$, and the linear energy $\mathcal{E}_\mathrm{L} = \mathcal{K} + \mathcal{V}_\mathrm{b}$. Here, the total energy is decomposed as $\mathcal{E} = \mathcal{K} + \mathcal{V}_\mathrm{b} + \mathcal{V}_\mathrm{s}$. (See Ref. [8] for details.) Note that the potential energy at each wavenumber $\mathcal{V}$ is decomposed into linear part, $\mathcal{V}_\mathrm{b}$, and nonlinear part, $\mathcal{V}_\mathrm{s}$, as $\mathcal{V} = \mathcal{V}_\mathrm{b} + \mathcal{V}_\mathrm{s}$, and the former (latter) takes large values in low- (high-)wavenumber range. The kinetic energy spectrum has flexion downward around $k \approx 200$. As a result, $\mathcal{E}$ as well as $\mathcal{E}_\mathrm{L}$ consists of two types of power law spectra with positive and negative exponents.

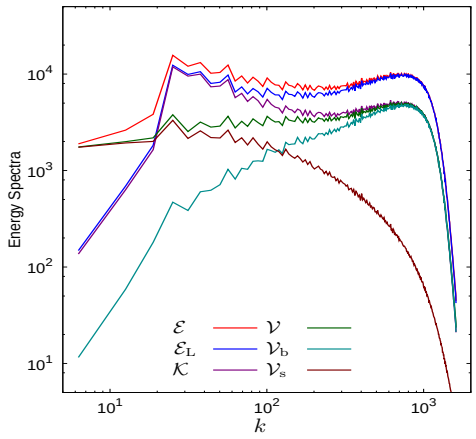

Figure 1. Azimuthally-integrated spectra of total and decomposed energies.

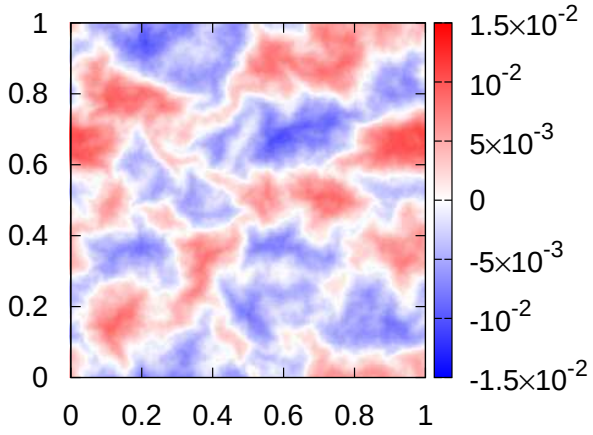

Figure 2. Field of lateral displacement.

Fig. 2 shows the real-space field of the lateral displacement ζ, whose structure has relatively large-scale. One might think that the field structure of ζ contradicts to $\mathcal{V}_b$ in Fig. 1, since the Fourier coefficient of the displacement $\zeta_{\boldsymbol{k}}$, whose dominant scale is large, determines the bending energy spectrum $V_{b\boldsymbol{k}} = \rho\omega_{\boldsymbol{k}}^2|\zeta_{\boldsymbol{k}}|^2/2$ as well as its azimuthally-integrated one $\mathcal{V}_b$, whose dominant scale is small. This is due to the fact that $\omega_{\boldsymbol{k}}$ is proportional to k^2,i.e., $V_{b\boldsymbol{k}} \propto k^4|\zeta_{\boldsymbol{k}}|^2$. The field looks like an intermediate state between the two fields reported in Fig. 2 of Ref. [9], which supports the adequacy of the energy level of the present simulation.

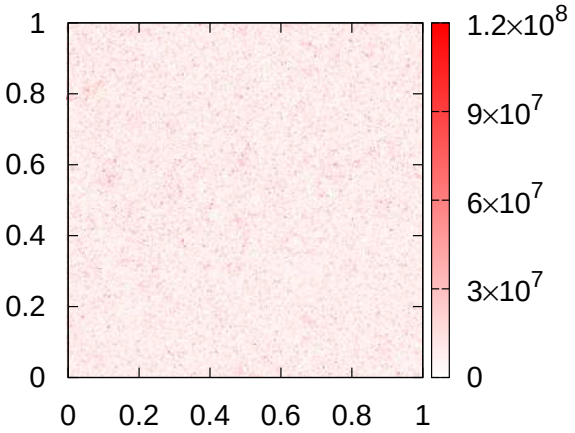

Figure 3. Field of total energy density.

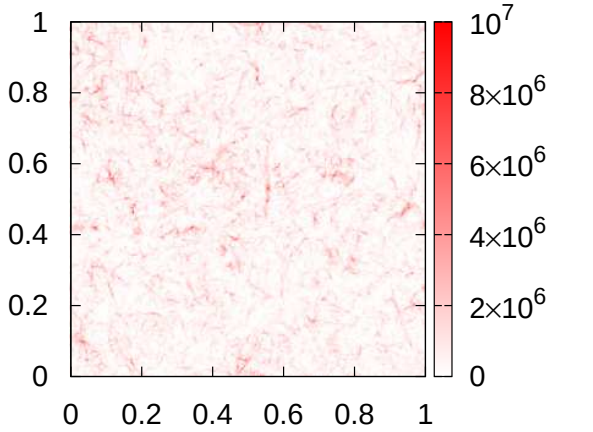

Figure 4. Field of stretching energy density.

On the contrary, the total energy density field shown in Fig. 3 has non-uniform distribution that consists of fine point-like structures. The total energy spectrum shown in Fig. 1 has two local maxima: one is located in low wavenumber $k \approx 8\pi$ and the other in high wavenumber $k \approx 256\pi$. Most of the energy is possessed by the latter high-wavenumber modes, since the number of the high-wavenumber modes is much larger than that of the low-wavenumber ones as known from the logarithmic scale of the horizontal axis. This fact as well as the random phase of weak turbulence in high wavenumber leads the fine-scale structures in the real space.

We also examined the fields of the kinetic energy K and the bending energy V_b, though the graphs are omitted. Both fields have similar fine-scale structures, while the dominant scales of

their spectra are different. It may be interesting to point out that the dominant scales of the spectra do not necessarily correspond to the characteristic scale in the real space. We must stress the importance of taking the phase correlations as well as the number of modes into account.

In Fig. 4, we find the ridge and the d-cone structures in the field of the stretching energy. It should be noted that the stretching energy stems from the nonlinearity of the FvK equation, which may induce the phase correlation of modes. It is also consistent with the stretching energy spectrum $\mathcal{V}_{\rm s}$ in Fig. 4, whose dominant scale is in low-wavenumber range.

3.2. Bundle structure and nonlinearity

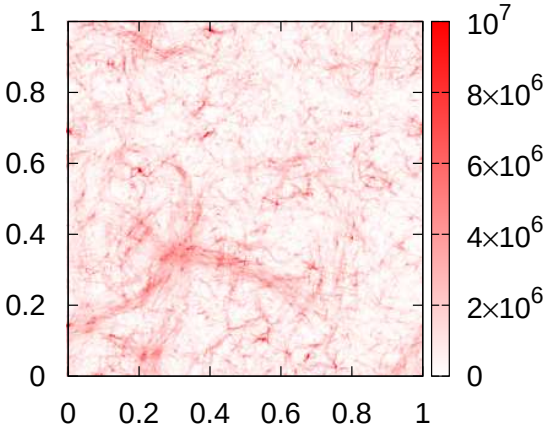

Figure 5. Bundle structure in the field of stretching energy density.

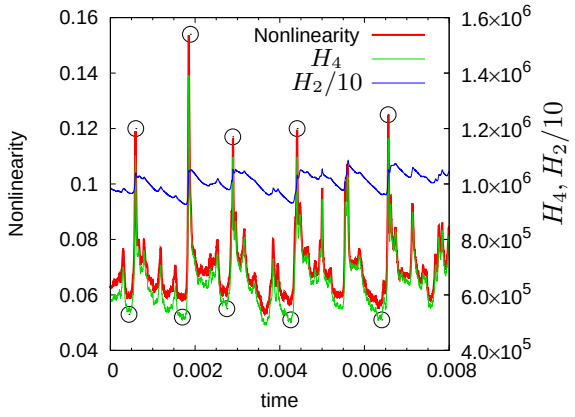

Figure 6. Time evolutions of nonlinearity (red), nonlinear (green) and linear (blue) energies. Circles show representative times.

We furthermore find that the *bundle* structures of the ridges, which are shown in Fig. 5, appear intermittently in the time evolution of the stretching energy field. The time evolution suggests the existence of active and moderate phases in the turbulent state. In Fig. 6 shown is the time evolution of nonlinearity, which is estimated by the ratio of the nonlinear energy to the linear energy, $\int \mathcal{V}_{\rm s} {\rm d}k / \int \mathcal{E}_{\rm L} {\rm d}k$, corresponding to the ratio of the quartic to quadratic order of the complex amplitude in Hamiltonian, H_4/H_2. The time evolutions of the nonlinear (green) and linear (blue) energies are also drawn in Fig. 6, where the linear energy is shifted downward by one decade. Quasi-periodic sawtooth behavior with mutually-synchronized phase is observed. Strong nonlinearity appears intermittently, while the nonlinearity always fluctuates randomly with relatively small amplitude. The bundle structures are observed at such active phases with the strong nonlinearity.

3.3. Probability distribution functions

Probability distribution functions (PDFs) are examined to characterize the statistical properties. Fig. 7, where the Gaussian PDF is also drawn for reference, shows the normalized PDFs of the lateral displacement ζ at five representative times respectively in active and moderate phases. As the representative times of active phase chosen are the times when the nonlinearity takes top five local maxima in Fig. 6, and the times 1.5×10^{-3} prior to these times are chosen as that of moderate phase. Although the fluctuation of the PDFs of ζ are large, one can safely say that the PDFs are almost Gaussian independent of the phases. The PDFs of p have little fluctuation and are well approximated by the Gaussian distribution, though the graphs are omitted here. The standard deviation of the lateral displacement ζ (the momentum p) in active phase is almost

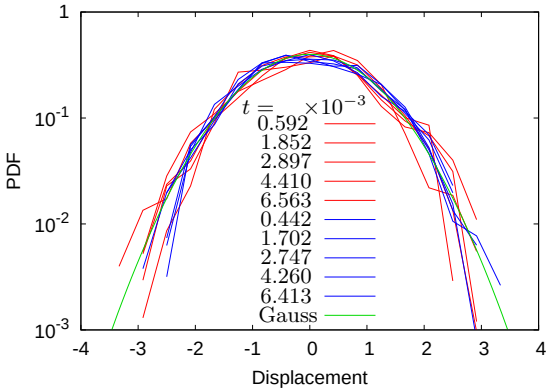

Figure 7. PDF of $\zeta(\boldsymbol{x})$ at active (red) and moderate (blue) phases and Gaussian (green).

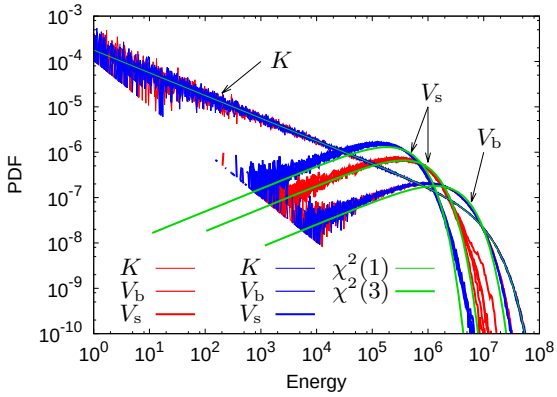

Figure 8. PDFs of $K(\boldsymbol{x})$, $V_{\rm b}(\boldsymbol{x})$ and $V_{\rm s}(\boldsymbol{x})$ at active (red) and moderate (blue) phases.

twice (the same as) that in moderate phase, which is consistent with the fact that most energy of the lateral displacement ζ (the momentum p) is in low- (high-)wavenumber range.

Fig. 8 shows the PDFs of the decomposed energies, K, $V_{\rm b}$ and $V_{\rm s}$ at the representative times. Since the momentum p is regarded as a random variable that obeys the Gaussian distribution with zero mean, the PDF of K is expected to obey the χ^2-distribution with 1-degree of freedom, $\chi^2(1)$, following from $K \propto p^2$. Since the expanded expressions of $V_{\rm b}$ and $V_{\rm s}$ in Eq. (2) respectively contain three quadratic terms and one cross term as $V_{\rm b} \propto \zeta_{xx}^2 + \zeta_{yy}^2 + 2(1-\nu)\zeta_{xy}^2 + 2\nu\zeta_{xx}\zeta_{yy}$ and $V_{\rm s} \propto \chi_{xx}^2 + \chi_{yy}^2 + 2(1+\nu)\chi_{xy}^2 - 2\nu\chi_{xx}\chi_{yy}$, the PDFs of $V_{\rm b}$ and $V_{\rm s}$ may be approximated by χ^2-distribution with 3-degrees of freedom, $\chi^2(3)$, under the assumption of the independency of the derivatives whose supports exist in high-wavenumber range. Although the distributions of linear energies, K and $V_{\rm b}$, are well approximated, that of $V_{\rm s}$ slightly deviate from $\chi^2(3)$ in the vicinity of $V_{\rm s} \sim 10^7$ where the nonlinearity is large. While the distributions of K and $V_{\rm b}$ are independent of the phases, that of $V_{\rm s}$ shifts according to the phases as seen in Fig. 8.

3.4. Nonlinear interactions among modes

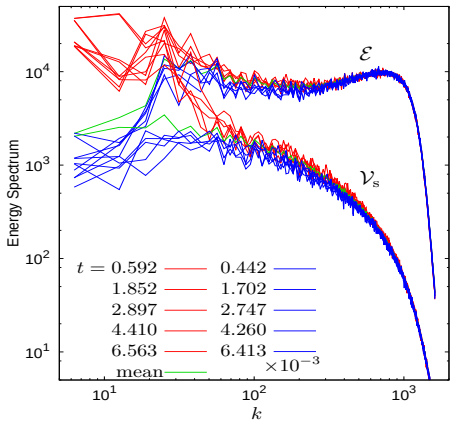

Figure 9. Representative energy spectra in active (red) and moderate (blue) phases.

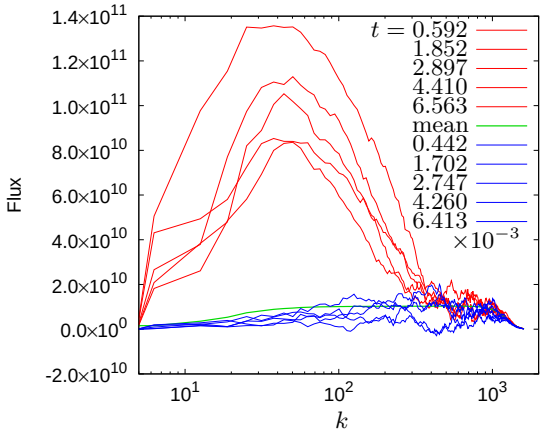

Figure 10. Representative energy fluxes in active (red) and moderate (blue) phases.

Fig. 9 shows the representatives of the total energy spectra $\mathcal{E}$ and the stretching energy $\mathcal{V}_s$ in both active and moderate phases. In low-wavenumber range, $k \lesssim 300$, the magnitudes of $\mathcal{E}$ in the active phases are relatively larger than those in the moderate phases, though they coincide in high-wavenumber range. The result is consistent with the PDF in the real space, shown in Fig. 8, since the linear energy dominates most of the total energy and remains unchanged in both phases. The difference appears more clearly in the curves of $\mathcal{V}_s$: the magnitudes of $\mathcal{V}_s$ in active phases in the forcing scale are almost one digit larger than those in moderate phases.

The fluxes of the total energy are also examined and shown at the representative times, since the nonlinear interaction among Fourier modes governs them. It should be noted here that these fluxes are different from the fluxes of linear energy which are conventionally used in WTT. The difference between those in the active and moderate phases is clearly seen in Fig. 10. The fluxes in the moderate phases can happen to take negative values in some wavenumber range. The fluxes in the active phases increase rapidly in low-wavenumber range, $k \lesssim 8\pi$, and decrease to around common value in relatively high-wavenumber range, $k \gtrsim 100\pi$, corresponding to the coincidence of the energy spectra in both phases as seen in Fig. 9. It means that the bundle structure observed in the real space is the embodiment of the strong nonlinear interactions among Fourier modes, which cause the energy input from the external force into the system.

4. Concluding Remark

We have investigated the real-space dynamics and the nonlinear interactions among Fourier modes in elastic wave turbulence by numerically simulating the Föppl-von Kármán equation. We find that the bundle structures of ridges appear intermittently in the time evolution of the stretching energy field, which is the nonlinear part of the total energy. The time evolution of the nonlinearity indicates the existence of active and moderate phases in turbulent state. Conditional sampling analysis to distinguish these phases reveals that the nonlinear interactions among modes behave differently depending on whether they are in active or moderate phases. The bundle structure, which stems from the strong nonlinear interactions, plays the essential role in supplying energy into the system. Some of the results, such as the bundle structures and the sawtooth behavior in Fig. 6, may depend on the forcing term adopted in the present work. It is our future work to examine their universality.

Acknowledgments

Numerical computation in this work was carried out at the Yukawa Institute Computer Facility. This work was partially supported by KAKENHI Grant No. 25400412.

References

[1] Landau L D and Lifshitz E M 1986 *Theory of Elasticity* (Butterworth-Heinemann, Oxford)
[2] Düring G, Josserand C and Rica S 2006 *Phys. Rev. Lett.* **97** 025003
[3] Boudaoud A, Cadot O, Odile B and Touzé C 2008 *Phys. Rev. Lett.* **100** 234504
[4] Mordant N 2008 *Phys. Rev. Lett.* **100** 234505
[5] Yokoyama N and Takaoka M 2013 *Phys. Rev. Lett.* **110** 105501
[6] Nazarenko S 2011 *Wave Turbulence* (Springer, Heidelberg)
[7] Yokoyama N and Takaoka M 2014 *Phys. Rev.* E **89** 012909
[8] Yokoyama N and Takaoka M (submitted to) *Phys. Rev.* E (arXiv:1407.1582 [nlin.CD])
[9] Miquel B, Alexakis A, Josserand C and Mordant N 2013 *Phys. Rev. Lett.* **111** 054302